

Superdirective dielectric spherical multilayer antennas

Roman Gaponenko,^{1,*} Alexander Moroz,² Iliia Rasskazov,³
Konstantin Ladutenko¹, Alexey Shcherbakov¹ and Pavel Belov,¹

¹ *Department of Physics and Engineering,
ITMO University, 197101, Saint-Petersburg, Russia*

² *Wave-scattering.com*

³ *The Institute of Optics, University of Rochester,
Rochester, New York 14627, United States*

* *Corresponding author: roman.gaponenko@metalab.ifmo.ru*

In the era of Internet of things, the emerging technologies require new generation of small form-factor, narrowband, and highly directive antennas to reduce the interference of radio-frequency waves. Here, on using a stochastic optimization algorithm combined with a rigorous analytic solution, we show that the classical directivity limit can be appreciably surpassed for electrically small dielectric resonant antennas. We provide experimentally feasible designs of superdirective multilayer spherical antennas excited by a point electric dipole.

The physical limitations on antennas are critical when designing efficient devices and they have been the subject of research since the early age of antenna science [1–3]. There is a trade-off between gain, G , which defines the spatial narrowness of radiation patterns, and the quality factor, Q , which characterizes the ratio of emitted power to the stored energy and is inversely proportional to the bandwidth when $Q \gg 1$ [4]. Gain is related to directivity, D , through $G = e_r D$, where e_r is the radiation efficiency of the antenna, taking into account antenna losses (it does not include polarization or impedance mismatch losses). In our study, we consider antennas without losses ($e_r = 1$). Therefore, we use only the term *directivity* in what follows without any loss of generality. The Harrington-Chu limit [2, 5] puts an upper bound on the directivity as $D_{\max} = (kR_{lim})^2 + 2kR_{lim}$, where R_{lim} is the radius of the sphere circumscribing an antenna and k is the free-space wave number. Kildal [6, 7] improved the formula for directivity limit in the case of small-size antennas to $D_{\max} = (kR_{lim})^2 + 3$. The above expressions for D_{\max} concern the so-called *normal* gain [5] and rely on the hypothesis which postulates a *linear* relationship between the antenna size and the number of spherical harmonic modes (see also the field degrees of freedom [8]) that can be efficiently excited by the antenna. The relation of the power radiated by the partial modes to the stored energy yields estimates on the quality factor, Q , and directivity, D [4, 9, 10]. However, the directivity is generally known to exceed these limits [1, 11]. The antennas with $D > D_{\max}$ are referred to as *superdirective*.

Recent publications [12–17] show continuing interest in overcoming the physical limitations on antenna design. Most of them are related to emerging applications and to advances in computer-based approaches to antenna optimization [18] as well as to numerical stability of theoretical treatments [19]. Since the superdirectivity of small antennas originates from their resonant behavior, it is accompanied by an ultranarrow-band response which lim-

its their applications. Nonetheless, the internet of things and wireless power transfer can benefit from such antennas in the radio frequency band [20]. In the optical band, high-index dielectric and plasmonic nanoparticles can be used to enhance the direction-selective absorption and emission of nanoantennas [21]. A convex optimization based on the method of moments developed in Ref. [22] was used to determine optimal surface currents which allowed both maximum gain and superdirective field patterns [23, 24] to be achieved. Although the proposed method is very general, it is unclear how to implement the optimal currents in antenna devices. Here, on using rigorous analytic treatment, we consider a spherical multilayer antenna with a dipole source excitation to demonstrate that particular superdirective designs with operation limits comparable to optimal current configurations [23] are possible even in a relatively simple geometry of small lossless dielectric resonant antennas.

We consider a lossless dielectric nonmagnetic concentric spherical multilayer antenna excited by an electric point dipole source, \mathbf{p} , located on the z -axis as shown in Fig. 1a. Because a dipole emits predominantly in a perpendicular direction to its axis, the radiation of a radially oriented dipole (i.e. parallel to the z -axis) is much more difficult to tailor by a nearby spherical antenna than for the tangential dipole orientation (i.e. perpendicular to the z -axis). For instance, for a radially oriented dipole outside the antenna, its radiation largely escapes to infinity without ever interacting with the antenna. Out of two possible orthogonal dipole orientations, we thus focus on the *tangential* dipole orientation (see Supplemental Material). The center of coordinates is at the sphere's origin. We denote the dipole position, r_d ; radii of layers, R_n (where $n = 1, \dots, N$); homogeneous isotropic concentric domains, Ω_n ; refractive indices of spherical layer domains, $\eta_n \geq 1$; refractive index of a surrounding medium, $\eta_{N+1} = 1$ (in the domain Ω_{N+1}). We consider non-magnetic materials with the permeability of a vacuum. Dipole locations both inside and outside of the spherical layers are allowed.

Maxwell's equations in each homogeneous layer can be solved via the vector spherical wave expansion of the electric field [25, Eq. (8)]:

$$\mathbf{E}_\gamma(n, \mathbf{r}) = \sum_L [A_{\gamma L}(n)\mathbf{J}_{\gamma L}(k_n, \mathbf{r}) + B_{\gamma L}(n)\mathbf{H}_{\gamma L}(k_n, \mathbf{r})], \quad (1)$$

where $\mathbf{J}_{\gamma L}$ and $\mathbf{H}_{\gamma L}$ are varieties of the vector multipoles $\mathbf{F}_{\gamma L}$ (see Eq. (A1) of Supplemental Material) which correspond to different linear combinations, $f_{\gamma l}$, of the spherical Bessel function in a given n -th shell [25]. Subscript γ denotes the polarization: $\gamma = M$ for magnetic, or transverse electric (TE) polarization, $\gamma = E$ for electric, or transverse magnetic (TM) polarization. The vector multipoles \mathbf{F}_{ML} and \mathbf{F}_{EL} reduce to \mathcal{M}_L and \mathcal{N}_L in the Stratton's notations [26, 27] provided that $f_{\gamma l}$ reduces to one of j_l or $h_l^{(1)}$. The index $L = (l, m)$ incorporates the orbital and magnetic quantum numbers, and i denotes the imaginary unit.

The continuity of tangential field components determines the interface conditions allowing to relate the expansion coefficients $A_{\gamma L}$ and $B_{\gamma L}$ in adjacent neighbouring regions Ω_n and Ω_{n+1} via 2×2 lowering $T_{\gamma L}^-$ or raising $T_{\gamma L}^+$ transfer matrices [25],

$$\begin{pmatrix} A_{\gamma L}(n+1) \\ B_{\gamma L}(n+1) \end{pmatrix} = T_{\gamma L}^+(n) \begin{pmatrix} A_{\gamma L}(n) \\ B_{\gamma L}(n) \end{pmatrix}, \quad (2)$$

$$\begin{pmatrix} A_{\gamma L}(n) \\ B_{\gamma L}(n) \end{pmatrix} = T_{\gamma L}^-(n) \begin{pmatrix} A_{\gamma L}(n+1) \\ B_{\gamma L}(n+1) \end{pmatrix}. \quad (3)$$

The transfer matrix method of Ref. [25] provides a means to calculate the emission of the dipole located either inside or in the vicinity of an arbitrary multilayered sphere. Two boundary conditions are required to unambiguously fix the solution. The so-called *regularity* boundary condition requires that the fields cannot be singular at the sphere core layer which, as in the case of Mie scattering from homogeneous spheres, requires that only $f_{\gamma l} \sim j_l$ are allowed in the core layer for $r < r_d$. Unlike the case of Mie scattering, the other boundary condition depends on the position of the radiating dipole. For the dipole outside of the multilayer sphere, the incoming dipole wave multipole coefficients $A_{\gamma L}(N+1)$ have to be the coefficients $\alpha_{\gamma L}^d$ of the electric field of a radiating dipole source located at a general position \mathbf{r}_d of a homogeneous space [28] [cf. Eq. (A9) of Supplemental Material]. For the dipole inside the multilayer sphere there is no incoming wave arriving from the outside, hence $A_{\gamma L}(N+1) \equiv 0$. However in the layer where the radiating dipole is located, the field expansion becomes [25]

$$\mathbf{E}(\mathbf{r}) = \begin{cases} \sum_{\gamma L} [(A_{\gamma L} + \alpha_{\gamma L}^d)\mathbf{J}_{\gamma L} + B_{\gamma L}\mathbf{H}_{\gamma L}], & r < r_d, \\ \sum_{\gamma L} [A_{\gamma L}\mathbf{J}_{\gamma L} + (B_{\gamma L} + \alpha_{\gamma L}^d)\mathbf{H}_{\gamma L}], & r > r_d, \end{cases} \quad (4)$$

with the amplitudes having a *discontinuity* at $r = r_d$, be-

cause such is the dipole field (cf. Eqs. (A6)-(A9) of the Supplemental Material). The quantity of crucial interest are the amplitudes $B_{\gamma L}(N+1)$ for $r > r_d$, which determine the radiating field escaping to infinity through the far-field amplitude matrix $\mathbf{F}(\theta, \varphi)$ (Eq. (A24) of the Supplemental Material). What is very convenient in the case of a multilayered sphere is that the $B_{\gamma L}(N+1)$'s can be represented in terms of *m-independent* linear combinations of the dipole field expansion coefficients $a_{\gamma L}^d$ and $\alpha_{\gamma L}^d$. The final solutions for $B_{\gamma L}(N+1)$ coefficients are strongly dependent on the position of the dipole source r_d . Four separate cases can be distinguished [25, Eqs. (60), (63), (65), (66)]:

- (a) for a dipole in a generic sphere shell different from the core and ambient

$$B_{\gamma L}(N+1) = \frac{\mathcal{T}_{11;\gamma l}\alpha_{\gamma L}^d + \mathcal{T}_{21;\gamma l}\alpha_{\gamma L}^d}{\mathcal{M}_{22;\gamma l}\mathcal{T}_{11;\gamma l} - \mathcal{M}_{12;\gamma l}\mathcal{T}_{21;\gamma l}}$$

- (b) for a dipole in the sphere core

$$B_{\gamma L}(N+1) = a_{\gamma L}^d / \mathcal{M}_{22;\gamma l}(1)$$

- (c) for a dipole outside the sphere with $r < r_d$

$$B_{\gamma L}(N+1) = [\mathcal{T}_{21;\gamma l}(N+1) / \mathcal{T}_{11;\gamma l}(N+1)] \alpha_{\gamma L}^d$$

- (d) for a dipole outside the sphere with $r > r_d$

$$B_{\gamma L}(N+1) = a_{\gamma L}^d + [\mathcal{T}_{21;\gamma l}(N+1) / \mathcal{T}_{11;\gamma l}(N+1)] \alpha_{\gamma L}^d,$$

where $\mathcal{T}_{\gamma L}(n) = \prod_{x=1}^{n-1} T_{\gamma L}^+(x)$ and $\mathcal{M}_{\gamma L}(n) = \prod_{x=n}^N T_{\gamma L}^-(x)$ are the ordered products of transfer matrices introduced formally by Eqs. (2) and (3).

Once the amplitudes $B_{\gamma L}(N+1)$ are known for $r > r_d$, the directivity in the direction specified by spherical angles (θ_0, φ_0) is determined by the formula:

$$D(\theta_0, \varphi_0) = \frac{4\pi r^2 |\mathbf{E}(\mathbf{r})|^2}{r^2 \oint |\mathbf{E}(\mathbf{r})|^2 d\Omega} \quad (5)$$

where $|\mathbf{E}(\mathbf{r})|^2$ and $\oint |\mathbf{E}(\mathbf{r})|^2 d\Omega$ can be expressed via coefficients $B_{\gamma L}(N+1)$ (see Supplemental Material). Therefore, the directivity $D(\theta_0, \varphi_0)$ depends on the geometrical and physical parameters of the problem R_n, η_n, r_d , the dipole polarization through the matrix elements of $\mathcal{T}_{\gamma L}, \mathcal{M}_{\gamma L}$ and also dipole amplitudes $a_{\gamma L}^d$ and $\alpha_{\gamma L}^d$.

In what follows, we shall use Eq. (5) for direct evaluation of the directivity in the optimization problem for determining maximum directivity $D(\theta_0, \varphi_0)$ for a given number of layers N within the following constraints:

1. bounded refractive indices $1 \leq \eta_n \leq \eta_{max}$ with fixed size parameter R_N/λ (see Fig. 1)
2. bounded size parameter $0 < kR_n \leq kR_{max}$ (see Fig. 2):

- for continuous range of refractive indices
 $1 \leq \eta_n \leq \eta_{max}$
- for a discrete set of refractive indices
 $\eta_n \in \{\eta^{(1)}, \eta^{(2)}, \dots\}$

The latter alternative is closer to possible practical implementations, since the set of materials available for fabrication is essentially limited (e.g., high-index ceramics in the radio-frequency band, or high-index dielectrics in the optical band), and it is instructive to compare optimization results in these two cases.

Since the convexity of Eq. (5) with respect to the optimization parameters is difficult to establish or check, we used a stochastic JADE algorithm [29] to maximize the directivity. This algorithm is an improved version of the differential evolution, which is effective for global optimization of functions with a large number of local peaks [29, 30] and, in particular, for problems associated with electromagnetic scattering [31]. For a convergence of the JADE optimization algorithm, one should select a sufficient parameters (population size, number of generations, crossover probability, etc), which strongly depend on Q -factor of the excited resonances: the higher the Q -factor, the greater these parameters must be. Moreover, a numerical implementation of the theoretical treatment presented above requires an accurate truncation of infinite sums to a limited number of terms. As discussed in [32] for spherical near-field antenna measurements, recommended number is $l_{max} = [kR_{lim}] + x_1$, where $[kR_{lim}]$ is an integer closest to the wavenumber k times the radius $R_{lim} = \max\{r_d; R_N\}$, and x_1 is an integer which depends on the position of the source and desired accuracy, wherein $x_1 = 10$ is sufficient for most of practical cases [33]. Nonetheless, the relation linking the size parameter with l_{max} is still questionable for electrically small resonant antennas.

The best possible theoretical directivity is given by the $\delta(\theta, \varphi)$ -function [34], which physical realization is a plane wave. In the case of the δ -function directivity, the expansion coefficients for the fields outside a sphere for $r > r_d$ have to be:

$$B_{\gamma l 1}(N+1) \sim i^l \sqrt{\frac{2l+1}{4\pi}} \quad (6)$$

(cf. plane wave expansion in Eq. (4.37) of Ref. [27]). The feasibility of this target, which imposes constraints on the geometry and material properties, is examined in Appendix A. It is shown there that the target can, in principle, be met only for the *tangential* dipole orientation. The coefficients (6) lead to the Harrington directivity limit $D_{max} = l_{max}(l_{max} + 2)$ [35] (cf. Eq. (A31)). Result (6), which can be seen as a generalization of the results of Ref. [34] for cylindrical geometry in two-dimensional space, is not bounded to a particular geometry and provides a recipe for an ultimate superdirective antenna design in three-dimensional space, useful for a range of applications.

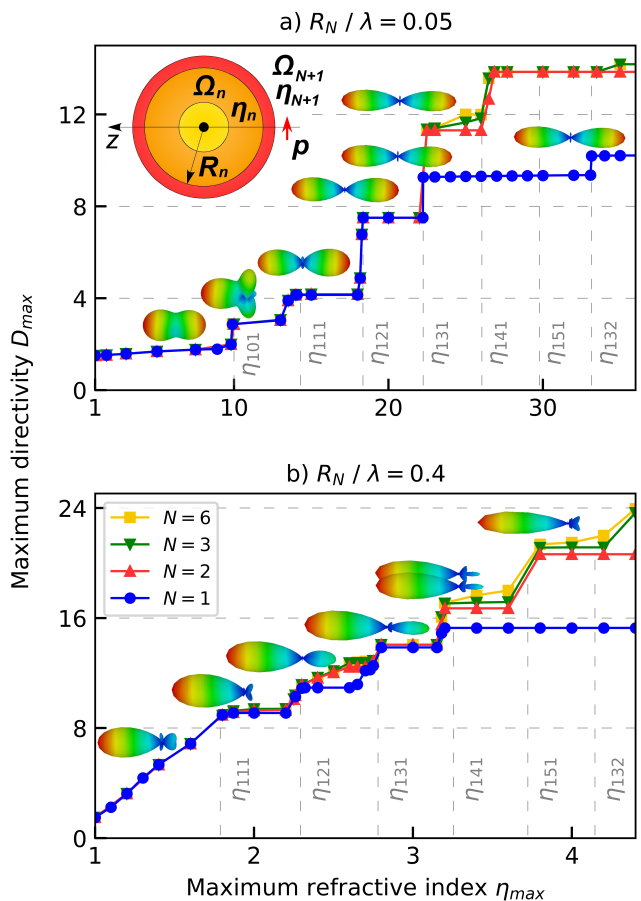


FIG. 1. Optimized directivity as a function of the maximum refractive index η_{max} for antennas with a different number of layers N . Sketch of the problem under the study is shown in inset in (a). The evolution of the radiation patterns for optimized designs is shown next to the key points on the graphs.

Dependence of optimized directivity on the refractive index for $R_N/\lambda = 0.05$ and 0.4 is shown in Fig. 1. The higher the ratio $\eta_{max}R_N/\lambda$ (which is proportional to an internal size parameter), the larger number of modes excited in the antenna. At the same time, the Q -factors of higher order modes are significantly higher. Jumps in directivity in the Fig. 1 are associated with the excitation of new modes in the dielectric sphere [36]. This is due to the leakage of the trapped electromagnetic field out of high refractive index dielectric scatterer into the environment, resulting in scattered field resonances (interaction between the polarization energy stored in the dielectric and the energy stored in the magnetic field [37]).

The approximate conditions for resonances of homogeneous spheres are provided by [37–39]:

$$\begin{cases} \eta_1 k R_1 \simeq r_{lp} & \text{for } \gamma = E \\ \eta_1 k R_1 \simeq r_{(l-1)p} & \text{for } \gamma = M \end{cases} \quad (7)$$

where r_{lp} is the p -th zero of the l -th order spherical Bessel

functions of the first kind, j_l ; η_1 and R_1 are refractive index and radius of a homogeneous spherical dielectric resonator. Since the condition for morphological Mie resonances of a homogeneous sphere (7) depends only on the values of product $\eta_1 k R_1$, the sphere radius R_1 can be decreased with the increase in refractive index while preserving the value of $\eta_1 k R_1$. Refractive indices of a homogeneous sphere η_{1lp} required for the first resonances are given in Table I.

Fig. 1 shows that the resonances of homogeneous sphere with the same $\eta_1 k R_1$ overlap for small refractive indices, while at larger index they become distinct (see also Fig. B1 in Appendix B). In the lossless case, there is a limit on the directivity for electrically small antennas which depends on the number of layers. According to our numerical results, the maximum directivity for a homogeneous sphere is achieved at $l = 3$. This can be explained by the fact that a single point electric dipole effectively excites modes only with $l \leq 3$ and is not efficient enough to excite higher modes of the homogeneous sphere. For $k R_1 \rightarrow 0$ we observe superdirective behavior near the resonance values r_{lp} with fixed $l = 3$. With increasing p , the directivity of the antenna continues to increase slightly: $D_{max} > 11.2$ for the resonances with $p > 14$ (see Table B1 in Appendix B), while the optimal dipole position moves slightly towards the outer layer.

Multilayer scatterers can provide higher directivity and have more complex resonance conditions, which can be derived through the poles of the directivity expression (5). Small multilayer sphere with $\eta_{max} k R_N < r_{31}$ usually converges to a homogeneous case (see Fig. 1). Even if there is a difference it is not notable. But above the discussed condition, directivity optimization results are different, since the additional internal layers can provide more efficient control over the field distribution and over the interference between different multipoles without changing the external size of the antenna. In the parameter region defined by $\eta_{max} k R_N > r_{51}$ it becomes difficult to obtain global maximum numerically using optimization procedure for multilayer spheres due to the large number of directivity peaks and their extremely high Q -factors (greater than 10^{10}). In this case,

| l, p | r_{lp} | $\eta_{1lp} = r_{lp}/kR_1$ |
|----------------|----------|----------------------------|
| $l = 0, p = 1$ | π | $0.5\lambda/R$ |
| $l = 1, p = 1$ | 4.4934 | $0.7151\lambda/R$ |
| $l = 2, p = 1$ | 5.7635 | $0.9173\lambda/R$ |
| $l = 3, p = 1$ | 6.9879 | $1.1122\lambda/R$ |
| $l = 4, p = 1$ | 8.1826 | $1.3024\lambda/R$ |
| $l = 2, p = 2$ | 9.0950 | $1.4475\lambda/R$ |
| $l = 5, p = 1$ | 9.3558 | $1.4890\lambda/R$ |
| $l = 3, p = 2$ | 10.4171 | $1.6579\lambda/R$ |
| $l = 6, p = 1$ | 10.5128 | $1.6732\lambda/R$ |

TABLE I. The first roots of the spherical Bessel functions and relative refractive indices corresponding to the resonances in the homogeneous sphere.

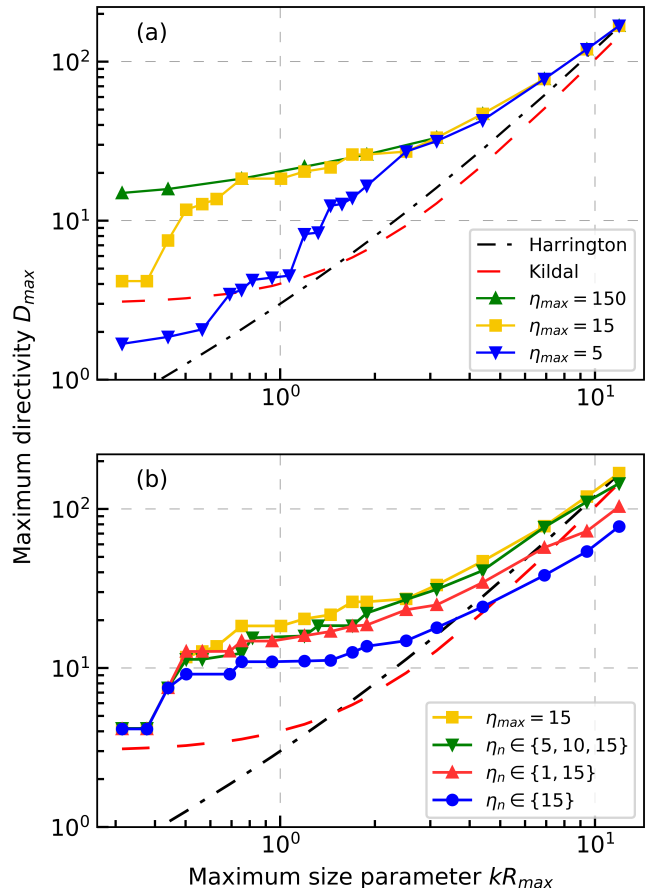


FIG. 2. Dependence of the optimized directivity on the size parameter kR_N for a spherical 3-layer antenna with a different limitation on a refractive index: (a) continuously varying; (b) discrete set.

stochastic optimization (i) is computationally expensive, (ii) not necessarily converges to a global maximum, and (iii) requires large number of initial populations and generations. There are various physical reasons which limit practically achievable Q -factor of antennas: surface roughness [40, 41], material imperfections, the presence of other objects in the immediate vicinity of the antenna, temperature of the environment, and challenging fabrication.

Fig. 2 demonstrates the dependence of the optimized directivity D_{max} on the antenna size parameter $0.3 \leq kR_N \leq 12$ for different limitations on the refractive index of a sphere η_{max} (taking into account high-index ceramics in the microwave band). Directivity behaves as a step function where the peaks correspond to the interference of the electric dipole with the various induced multipoles of the sphere (either magnetic or electric). The optimal directivity is almost independent on the formulation of the optimization problem for sufficiently large sets of available refractive indices as demonstrated in Fig. 2b. D_{max} depends not only on the number of terms in a set, but also on the available refractive indices.

An example of optimization for a homogeneous sphere is presented in Appendix B. Several optimized designs of homogeneous and multilayer spherical superdirective antennas are presented in Appendix C. The resulting designs for $kR_N \rightarrow 0$ are generally forward-backward, while as kR_N increases, the *forward* direction becomes dominant due to the interference between different modes (see Fig. 1). Occasionally, more complex shapes can be obtained, because optimization is performed in the specified direction $\theta = 0^\circ$ and does not control the field distribution in other directions.

In conclusion, we have shown that, using dielectric materials for electrically small resonant antennas, the classical limit for directivity can be overcome. We presented (i) a number of superdirective antenna designs and (ii) a stochastic optimization-based recipe to construct new superdirective antennas of a given size and materials. We have also provided a rigorous derivation of the maximum

directivity, D_{\max} , for the ultimate superdirective antenna design. Our performance analysis revealed that, as the size of antenna decreases, it is essential to use high refractive index materials in order to obtain a superdirective antenna radiation pattern. An important property of the proposed designs is their geometrical simplicity: a multilayer sphere excited by a point dipole. It is anticipated that multiple dipole feeds will be capable of communicating with multiple receiver devices simultaneously using highly directive beams without any mechanical rearrangement. We hope that the results presented here could be applied in the development of subwavelength resonant dielectric antennas for the internet of things and other wireless applications. Moreover, our results can be easily adapted for other cases, such as lossy metal materials, which are of significant interest [34] for fluorescence collection and quantum optics, and are the subject of further study.

-
- [1] C. J. Bouwkamp and N. G. de Bruijn, The problem of optimum antenna current distribution, Philips Res. Rep **1**, 135 (1945).
- [2] L. J. Chu, Physical Limitations of Omni-Directional Antennas, J. Appl. Phys. **19**, 1163 (1948).
- [3] H. Riblet, Note on the Maximum Directivity of an Antenna, Proc. IRE **36**, 620 (1948).
- [4] R. Hansen, Fundamental limitations in antennas, Proc. IEEE **69**, 170 (1981).
- [5] R. F. Harrington, On the Gain and Beamwidth of Directional Antennas, IRE Transactions on Antennas and Propagation (1958).
- [6] P.-S. Kildal, Fundamental directivity and efficiency limitations of single- and multi-port antennas, in *2nd European Conference on Antennas and Propagation (EuCAP 2007)* (Institution of Engineering and Technology, Edinburgh, UK, 2007) pp. 396–396.
- [7] P.-S. Kildal, E. Martini, and S. Maci, Degrees of Freedom and Maximum Directivity of Antennas: A bound on maximum directivity of nonsuperreactive antennas., IEEE Antennas Propag. Mag. **59**, 16 (2017).
- [8] O. M. Bucci and G. Franceschetti, On the degrees of freedom of scattered fields, IEEE Trans. Antennas Propagat. **37**, 918 (1989).
- [9] W. Geyi, Physical limitations of antenna, IEEE Trans. Antennas Propagat. **51**, 2116 (2003).
- [10] R. Collin and S. Rothschild, Evaluation of antenna Q, IEEE Trans. Antennas Propagat. **12**, 23 (1964).
- [11] A. Uzkov, An approach to the problem of optimum directive antenna design, in *Comptes Rendus (Doklady) de l'Academie des Sciences de l'URSS*, Vol. 53 (1946) pp. 35–38.
- [12] M. Pigeon, C. Delaveaud, L. Rudant, and K. Belmekdem, Miniature directive antennas, Int. J. Microw. Wirel. T. **6**, 45 (2014).
- [13] B. Jonsson, S. Shi, L. Wang, F. Ferrero, and L. Lizzi, On Methods to Determine Bounds on the Q-Factor for a Given Directivity, IEEE Trans. Antennas Propagat. **65**, 5686 (2017).
- [14] C. Pfeiffer, Fundamental Efficiency Limits for Small Metallic Antennas, IEEE Trans. Antennas Propagat. **65**, 1642 (2017).
- [15] M. Shahpari and D. V. Thiel, Fundamental Limitations for Antenna Radiation Efficiency, IEEE Trans. Antennas Propagat. **66**, 3894 (2018).
- [16] L. Jelinek, K. Schab, and M. Capek, Radiation Efficiency Cost of Resonance Tuning, IEEE Trans. Antennas Propagat. **66**, 6716 (2018).
- [17] W. Chen, J. Fu, Q. Wu, and B. Lv, Design principle of cylindrical superdirective antenna, J. Phys. D **52**, 495102 (2019).
- [18] A. Karlsson, On the Efficiency and Gain of Antennas, PIER **136**, 479 (2013).
- [19] M. Majic and E. C. Le Ru, Numerically stable formulation of Mie theory for an emitter close to a sphere, Appl. Opt. **59**, 1293 (2020).
- [20] W. Lin, R. W. Ziolkowski, and J. Huang, Electrically Small, Low-Profile, Highly Efficient, Huygens Dipole Rectennas for Wirelessly Powering Internet-of-Things Devices, IEEE Trans. Antennas Propagat. **67**, 3670 (2019).
- [21] R. W. Ziolkowski, Using Huygens Multipole Arrays to Realize Unidirectional Needle-Like Radiation, Phys. Rev. X **7**, 031017 (2017).
- [22] M. Gustafsson and S. Nordebo, Optimal Antenna Currents for Q, Superdirectivity, and Radiation Patterns Using Convex Optimization, IEEE Trans. Antennas Propagat. **61**, 1109 (2013).
- [23] M. Gustafsson and M. Capek, Maximum Gain, Effective Area, and Directivity, IEEE Trans. Antennas Propagat. **67**, 5282 (2019).
- [24] M. Gustafsson, M. Capek, and K. Schab, Tradeoff Between Antenna Efficiency and Q-Factor, IEEE Trans. Antennas Propagat. **67**, 2482 (2019).
- [25] A. Moroz, A recursive transfer-matrix solution for a dipole radiating inside and outside a stratified sphere, Ann. Phys. **315**, 352 (2005).
- [26] J. Stratton, *Electromagnetics Theory* (McGraw-Hill, 1941).
- [27] C. F. Bohren and D. R. Huffman, *Absorption and Scat-*

- tering of Light by Small Particles (John Wiley & Sons, 1998).
- [28] H. Chew, P. J. McNulty, and M. Kerker, Model for Raman and fluorescent scattering by molecules embedded in small particles, *Phys. Rev. A* **13**, 396 (1976).
- [29] J. Zhang and A. C. Sanderson, JADE: Adaptive differential evolution with optional external archive, *IEEE Trans. on Evolutionary Comput.* **13**, 945 (2009).
- [30] M. Yang, Z. Cai, C. Li, and J. Guan, An improved JADE algorithm for global optimization, in *Proceedings of the 2014 IEEE Congress on Evolutionary Computation, CEC 2014* (2014).
- [31] K. Ladutenko, P.-R. Ovidio, I. Melchakova, I. Yagupov, and P. Belov, Reduction of scattering using thin all-dielectric shells designed by stochastic optimizer, *J. Appl. Phys.* **116**, 184508 (2014).
- [32] IEEE Standards Association, IEEE Recommended Practice for Near-Field Antenna Measurements (2012).
- [33] J. E. Hansen, *Spherical Near-field Antenna Measurements* (IEEE, 1988).
- [34] S. Arslanagić and R. W. Ziolkowski, Highly subwavelength, superdirective cylindrical nanoantenna, *Phys. Rev. Lett.* **120**, 237401 (2018).
- [35] R. F. Harrington, Effect of antenna size on gain, bandwidth, and efficiency, *J. Res. Natl. Bur. Stand. Sec. D* **64D**, 1 (1960).
- [36] M. Gastine, L. Courtois, and J. L. Dormann, Electromagnetic Resonances of Free Dielectric Spheres, *IEEE Trans. Microwave Theory Tech.* **15**, 694 (1967).
- [37] C. Forestiere, G. Miano, G. Rubinacci, M. Pascale, A. Tamburrino, R. Tricarico, and S. Ventre, Magnetoquasistatic resonances of small dielectric objects, *Phys. Rev. Research* **2**, 013158 (2020).
- [38] C. C. Lam, P. T. Leung, and K. Young, Explicit asymptotic formulas for the positions, widths, and strengths of resonances in Mie scattering, *J. Opt. Soc. Am. B* **9**, 1585 (1992).
- [39] C. A. Balanis, *Advanced engineering electromagnetics*, 2nd ed. (John Wiley & Sons, Inc., 2012).
- [40] G. Farias, E. Vasconcelos, S. Cesar, and A. Maradudin, Mie scattering by a perfectly conducting sphere with a rough surface, *Physica A* **207**, 315 (1994).
- [41] C. Li, G. W. Kattawar, and P. Yang, Effects of surface roughness on light scattering by small particles, *J. Quant. Spectrosc. Radiat. Transfer* **89**, 123 (2004).
- [42] A. Edmonds, *Angular Momentum in Quantum Mechanics*, Investigations in physics (Princeton University Press, 1960).
- [43] M. I. Mishchenko, Light scattering by randomly oriented axially symmetric particles, *J. Opt. Soc. Am. A* **8**, 871 (1991).
- [44] H. Chew, Transition rates of atoms near spherical surfaces, *J. Chem. Phys.* **87**, 1355 (1987).
- [45] H. Chew, Radiation and lifetimes of atoms inside dielectric particles, *Phys. Rev. A* **38**, 3410 (1988).
- [46] F. W. Olver, D. W. Lozier, R. F. Boisvert, and C. W. Clark, *NIST Handbook of Mathematical Functions*, 1st ed. (Cambridge University Press, 2010).
- [47] A. P. Prudnikov, Y. A. Brychkov, and O. I. Marichev, *Integrals and series. Volume 3: More special functions* (New York: Gordon and Breach Science Publishers, 1990) p. 800.
- [48] M. Abramowitz and I. A. Stegun, *Handbook of Mathematical Functions* (Dover Publications, New York, 1973) p. 1046.
- [49] M. Kerker, D.-S. Wang, and H. Chew, Surface enhanced Raman scattering (SERS) by molecules adsorbed at spherical particles, *Appl. Opt.* **19**, 3373 (1980).

Appendix A: Theoretical part

1. Special values of the vector spherical harmonics and dipole field expansion coefficients on the z -axis

Normalized transverse vector multipoles are defined as

$$\begin{aligned}\mathbf{F}_{ML}(k_n, \mathbf{r}) &= f_{ML}(k_n r) \mathbf{Y}_L^{(m)}(\mathbf{r}), \\ \mathbf{F}_{EL}(k_n, \mathbf{r}) &= \frac{1}{k_n r} \left\{ \sqrt{l(l+1)} f_{EL}(k_n r) \mathbf{Y}_L^{(o)}(\mathbf{r}) \right. \\ &\quad \left. + (r f_{EL})'(k_n r) \mathbf{Y}_L^{(e)}(\mathbf{r}) \right\},\end{aligned}\quad (\text{A1})$$

where $f_{\gamma L}$ is an arbitrary linear combination of spherical Bessel functions, $\mathbf{Y}_L^{(a)}$ are vector spherical harmonics, and L is a composite angular momentum index, $L = (l, m)$, where the respective $l \geq 1$ and m label the orbital and magnetic angular numbers, and prime denotes the radial derivative d/dr . In what follows it is expedient to introduce scalar angular functions,

$$\pi_{ml}(\theta) = \frac{m}{\sin \theta} d_{0m}^l(\theta), \quad \tau_{ml}(\theta) = \frac{d}{d\theta} d_{0m}^l(\theta), \quad (\text{A2})$$

which are defined in terms of the Wigner d -functions d_{0m}^l [42] and which can all be generated by stable recurrences. Then

$$\begin{aligned}\mathbf{Y}_L^{(m)} &= (-1)^m i d_l \left(i \hat{\theta} \pi_{ml} - \hat{\varphi} \tau_{ml} \right) e^{im\varphi}, \\ \mathbf{Y}_L^{(e)} &= (-1)^m i d_l \left(\hat{\theta} \tau_{ml} + i \hat{\varphi} \pi_{ml} \right) e^{im\varphi}, \\ \mathbf{Y}_L^{(o)} &= i \hat{r} Y_L \\ &= i \gamma'_L P_l^m(\cos \theta) e^{im\varphi} \hat{\mathbf{r}} \\ &= (-1)^m i \sqrt{l(l+1)} d_l d_{0m}^l(\theta) e^{im\varphi} \hat{\mathbf{r}} \\ &= i \gamma'_L \mathbf{P}_L(\theta, \varphi).\end{aligned}\quad (\text{A3})$$

\mathbf{C} , \mathbf{B} , and \mathbf{P} in the Mishchenko notation [43] are

$$\begin{aligned}\mathbf{C}_L(\theta) &= \mathbf{e}_\theta \frac{im}{\sin \theta} d_{0m}^l(\theta) - \mathbf{e}_\varphi \frac{dd_{0m}^l(\theta)}{d\theta}, \\ \mathbf{B}_L(\theta) &= \mathbf{e}_\theta \frac{dd_{0m}^l(\theta)}{d\theta} + \mathbf{e}_\varphi \frac{im}{\sin \theta} d_{0m}^l(\theta) = \mathbf{r}_0 \times \mathbf{C}_L, \\ \mathbf{P}_L(\theta) &= \frac{\mathbf{r}}{r} d_{0m}^l(\theta).\end{aligned}\quad (\text{A4})$$

Eq. (4.2.3) of [42] for the special case $\beta = \theta = 0$ and $m' = 0$ yields

$$d_{0m}^l(0) = (-1)^m \delta_{0m} = \delta_{m0}. \quad (\text{A5})$$

It should be remembered though that Edmonds d_{0m}^l are related to our up to prefactor of $(-1)^m$. However, because of δ_{0m} , the latter factor does not play any role in the above identities.

The electric field at \mathbf{r} due to an electric dipole \mathbf{p} at \mathbf{r}_d radiating at frequency ω in a medium with ε , μ is given

for $r > r_d$ by [44]

$$\begin{aligned}\mathbf{E}_d(\mathbf{r}) &= \sum_L \left[a_{ML}^d \mathbf{H}_{ML}(k, \mathbf{r}) + a_{EL}^d \mathbf{H}_{EL}(k, \mathbf{r}) \right], \\ \mathbf{H}_d(\mathbf{r}) &= -i \sqrt{\frac{\varepsilon}{\mu}} \sum_L \left[a_{ML}^d \mathbf{H}_{EL}(k, \mathbf{r}) + a_{EL}^d \mathbf{H}_{ML}(k, \mathbf{r}) \right],\end{aligned}\quad (\text{A6})$$

where $l \geq 1$ and [25, Eq. (44)]

$$\begin{aligned}a_{ML}^d &= 4\pi i (k^3/\varepsilon) \mathbf{p} \cdot \mathbf{J}_{ML}^*(k, \mathbf{r}_d), \\ a_{EL}^d &= 4\pi i (k^3/\eta) \sqrt{\frac{\mu}{\varepsilon}} \mathbf{p} \cdot \mathbf{J}_{EL}^*(k, \mathbf{r}_d) \\ &= 4\pi i (k^3/\varepsilon) \mathbf{p} \cdot \mathbf{J}_{EL}^*(k, \mathbf{r}_d),\end{aligned}\quad (\text{A7})$$

k being the wave vector in the medium where the dipole is embedded. For $r < r_d$, one interchanges j_l and $h_l^{(1)}$ and has

$$\begin{aligned}\mathbf{E}_d(\mathbf{r}) &= \sum_L \left[\alpha_{ML}^d \mathbf{J}_{ML}(k, \mathbf{r}) + \alpha_{EL}^d \mathbf{J}_{EL}(k, \mathbf{r}) \right], \\ \mathbf{H}_d(\mathbf{r}) &= -i \sqrt{\frac{\varepsilon}{\mu}} \sum_L \left[\alpha_{ML}^d \mathbf{J}_{EL}(k, \mathbf{r}) + \alpha_{EL}^d \mathbf{J}_{ML}(k, \mathbf{r}) \right],\end{aligned}\quad (\text{A8})$$

where [25, Eq. (46)]

$$\begin{aligned}\alpha_{ML}^d &= 4\pi i (k^3/\varepsilon) \mathbf{p} \cdot \mathbf{H}_{ML}^*(k, \mathbf{r}_d), \\ \alpha_{EL}^d &= 4\pi i (k^3/n) \sqrt{\frac{\mu}{\varepsilon}} \mathbf{p} \cdot \mathbf{H}_{EL}^*(k, \mathbf{r}_d) \\ &= 4\pi i (k^3/\varepsilon) \mathbf{p} \cdot \mathbf{H}_{EL}^*(k, \mathbf{r}_d).\end{aligned}\quad (\text{A9})$$

To avoid confusion, star here and in Eq. (A7) above denotes the complex conjugation which only applies to the vector spherical harmonics and not to the spherical Bessel functions [44, 45].

In what follows, the above formulas (A3) for vector spherical harmonics will be used in reducing the electric dipole fields (A6) and (A8) for the special case when the dipole is located on the z -axis.

$$a. \quad \theta = 0$$

According to Eqs. (4.1-4) of [43] (cited therein as formulae of D. A. Varshalovich, A. N. Moskalev, and V. K. Khersonskij, *Quantum Theory of Angular Momentum* (Nauka, Leningrad, 1975))

$$\begin{aligned}\pi_{ml}(0) &= \frac{\delta_{m,\pm 1}}{2} \sqrt{l(l+1)}, \\ \tau_{ml}(0) &= \frac{m \delta_{m,\pm 1}}{2} \sqrt{l(l+1)}.\end{aligned}\quad (\text{A10})$$

On substituting the special values (A5) of the Wigner functions and (A10) in (A4), one finds

$$\begin{aligned}\mathbf{C}_L(0) &= \frac{\sqrt{l(l+1)}}{2} (i\mathbf{e}_\theta - m\mathbf{e}_\phi)\delta_{m,\pm 1}, \\ \mathbf{B}_L(0) &= \frac{\sqrt{l(l+1)}}{2} (m\mathbf{e}_\theta + i\mathbf{e}_\phi)\delta_{m,\pm 1}, \\ \mathbf{P}_L(0) &= \hat{\mathbf{z}}\delta_{m0}.\end{aligned}$$

The values of the vector spherical harmonics in (A3) for \mathbf{r} on the positive z -axis follow directly on multiplying the above results by the factor $i(-1)^m d_l$, and additionally by $\sqrt{l(l+1)}$ for $\mathbf{Y}_L^{(o)}$, resulting in

$$\begin{aligned}\mathbf{Y}_L^{(m)}(\hat{\mathbf{z}}) &= -i\sqrt{\frac{2l+1}{4\pi}} \frac{\delta_{m,\pm 1}}{2} (i\mathbf{e}_\theta - m\mathbf{e}_\phi) e^{im\varphi} \\ &= \frac{\delta_{m,\pm 1}}{2} \sqrt{\frac{2l+1}{4\pi}} (\mathbf{e}_\theta + im\mathbf{e}_\phi) e^{im\varphi}, \\ \mathbf{Y}_L^{(e)}(\hat{\mathbf{z}}) &= -i\sqrt{\frac{2l+1}{4\pi}} \frac{\delta_{m,\pm 1}}{2} (m\mathbf{e}_\theta + i\mathbf{e}_\phi) e^{im\varphi} \\ &= \frac{\delta_{m,\pm 1}}{2} \sqrt{\frac{2l+1}{4\pi}} (-im\mathbf{e}_\theta + \mathbf{e}_\phi) e^{im\varphi}, \\ \mathbf{Y}_L^{(o)}(\hat{\mathbf{z}}) &= i\delta_{m0} \sqrt{\frac{2l+1}{4\pi}} \hat{\mathbf{z}}.\end{aligned}\quad (\text{A11})$$

One can easily verify that general relations $\mathbf{Y}_L^{(c)*} = -(-1)^m \mathbf{Y}_{l,-m}^{(c)}$ hold for the special values. The above values in spherical coordinates can be translated into those in Cartesian coordinates on using elementary relations

$$\begin{aligned}\mathbf{e}_z &= \cos\theta \mathbf{e}_r - \sin\theta \mathbf{e}_\theta, \\ \mathbf{e}_\rho &= \sin\theta \mathbf{e}_r + \cos\theta \mathbf{e}_\theta, \\ \mathbf{e}_x &= \cos\varphi \mathbf{e}_\rho - \sin\varphi \mathbf{e}_\varphi, \\ \mathbf{e}_y &= \sin\varphi \mathbf{e}_\rho + \cos\varphi \mathbf{e}_\varphi.\end{aligned}$$

For a dipole located on the z -axis in the $\phi = 0$ plane we have two possible orientations: along either (i) \mathbf{e}_θ (i.e. tangential) or (ii) \mathbf{e}_r (i.e. radial). In the former case, on making use of Eq. (3) of Ref. [25] and (A11), the dipole field expansion coefficients $a_{\gamma L}^d$ of Eq. (A7) become

$$\begin{aligned}a_{ML}^d &= i\delta_{m,\pm 1} \left[\sqrt{(2l+1)\pi} (k_d^3/\varepsilon_d) p_\theta \right] j_l(k_d r_d), \\ a_{EL}^d &= m\delta_{m,\pm 1} \left[\sqrt{(2l+1)\pi} (k_d^3/\varepsilon_d) p_\theta \right] \frac{[r j_l(k_d r_d)]'}{k_d r_d},\end{aligned}\quad (\text{A12})$$

where $l \geq 1$, with k_d being the wave vector and ε_d the dielectric constant in the medium where the dipole is embedded, and r_d the radial position of the dipole on the z -axis.

In the case of the dipole oriented along \mathbf{e}_r , the dipole

expansion coefficients $a_{\gamma L}^d$ of Eq. (A7) become

$$\begin{aligned}a_{ML}^d &= 0, \\ a_{EL}^d &= \delta_{m0} \left[\sqrt{4l(l+1)(2l+1)\pi} (k_d^3/\varepsilon_d) p_r \right] \frac{j_l(k_d r_d)}{k_d r_d}.\end{aligned}\quad (\text{A13})$$

The dipole field expansion coefficients $\alpha_{\gamma L}^d$ of Eq. (A9) are readily obtained by substituting $h_l^{(1)}$ for j_l in the above expressions (A12), (A13). The expressions in square brackets therein are common prefactors. The ‘‘missing’’ i -factor in the expression (A12) for a_{EL}^d compared to that for a_{ML}^d is later compensated by D_{EL} being multiplied by i in Eqs. (A23), (A24) and in Eq. (85) of Ref. [25].

b. $\theta = \pi$

One has (Eqs. (4.2.4) and (4.2.6) of Ref. [42])

$$d_{0m}^l(\pi - \beta) = (-1)^{l+m} d_{0m}^l(\beta),$$

and the following relations

$$\begin{aligned}\pi_{ml}(\pi - \beta) &= (-1)^{l+m} \pi_{ml}(\beta), \\ \tau_{ml}(\pi - \beta) &= -(-1)^{l+m} \tau_{ml}(\beta).\end{aligned}$$

The relations generalize the earlier relations of Bohren & Huffman [27] (see Eq. (4.48) therein) that are valid in the special case of $m = 1$. On substituting the above relations for $\beta = 0$,

$$\begin{aligned}d_{0m}^l(\pi) &= (-1)^l \delta_{0m}, \\ \pi_{ml}(\pi) &= (-1)^{l+m} \frac{\delta_{m,\pm 1}}{2} \sqrt{l(l+1)}, \\ \tau_{ml}(\pi) &= -(-1)^{l+m} \frac{m\delta_{m,\pm 1}}{2} \sqrt{l(l+1)},\end{aligned}$$

where the first relation is equivalent to $P_l(-1) = (-1)^l P_l(1) = (-1)^l$, into (A4),

$$\begin{aligned}\mathbf{C}_L(\pi) &= (-1)^{l+m} \frac{\sqrt{l(l+1)}}{2} (i\mathbf{e}_\theta + m\mathbf{e}_\phi) \delta_{m,\pm 1}, \\ \mathbf{B}_L(\pi) &= (-1)^{l+m} \frac{\sqrt{l(l+1)}}{2} (-m\mathbf{e}_\theta + i\mathbf{e}_\phi) \delta_{m,\pm 1}, \\ \mathbf{P}_L(\pi) &= (-1)^l \hat{\mathbf{z}} \delta_{m0}.\end{aligned}$$

In view of the definitions (A.5) of Ref. [25] [note that the prefactor $(-1)^m$ there cancels against that in $(-1)^{l+m}$ above],

$$\begin{aligned}\mathbf{Y}_L^{(m)}(-\hat{\mathbf{z}}) &= i(-1)^l \sqrt{\frac{2l+1}{4\pi}} \frac{\delta_{m,\pm 1}}{2} (i\mathbf{e}_\theta + m\mathbf{e}_\phi) e^{im\varphi} \\ &= (-1)^l \frac{\delta_{m,\pm 1}}{2} \sqrt{\frac{2l+1}{4\pi}} (-\mathbf{e}_\theta + im\mathbf{e}_\phi) e^{im\varphi},\end{aligned}$$

$$\begin{aligned}
\mathbf{Y}_L^{(e)}(-\hat{\mathbf{z}}) &= i(-1)^l \sqrt{\frac{2l+1}{4\pi}} \frac{\delta_{m,\pm 1}}{2} (-m\mathbf{e}_\theta + i\mathbf{e}_\phi) e^{im\varphi} \\
&= -(-1)^l \frac{\delta_{m,\pm 1}}{2} \sqrt{\frac{2l+1}{4\pi}} (ime_\theta + \mathbf{e}_\phi) e^{im\varphi}, \\
\mathbf{Y}_L^{(o)}(-\hat{\mathbf{z}}) &= i(-1)^l \delta_{m0} \sqrt{\frac{2l+1}{4\pi}} \hat{\mathbf{z}}. \tag{A14}
\end{aligned}$$

Thus for a dipole located on the negative z -axis in the $\phi = 0$ plane along \mathbf{e}_θ , the dipole field expansion coefficients $a_{\gamma L}^d$ of Eq. (A7) become on making use of Eq. (3) of Ref. [25] and Eq. (A14)

$$\begin{aligned}
a_{ML}^d &= -i(-1)^l \delta_{m,\pm 1} \left[\sqrt{(2l+1)\pi} (k_d^3/\varepsilon_d) p_\theta \right] j_l(k_d r_d), \\
a_{EL}^d &= -m(-1)^l \delta_{m,\pm 1} \left[\sqrt{(2l+1)\pi} (k_d^3/\varepsilon_d) p_\theta \right] \frac{[r j_l(k_d r_d)]'}{k_d r_d}. \tag{A15}
\end{aligned}$$

For the dipole oriented along \mathbf{e}_r , the dipole expansion coefficients $a_{\gamma L}^d$ of Eq. (A7) become

$$\begin{aligned}
a_{ML}^d &= 0, \\
a_{EL}^d &= (-1)^l \delta_{m0} \left[\sqrt{4l(l+1)(2l+1)\pi} (k_d^3/\varepsilon_d) p_r \right] \frac{j_l(k_d r_d)}{k_d r_d}. \tag{A16}
\end{aligned}$$

The factor $(-1)^l$ in the above expressions (A14), (A15), (A16) can be seen as resulting from the *spatial inversion* $\mathbf{n} \rightarrow -\mathbf{n}$ of the scalar spherical harmonics,

$$Y_{lm}(-\mathbf{n}) = (-1)^l Y_{lm}(\mathbf{n}),$$

in agreement with the *reflection formula* [46, (14.7.17)], [47, Appendix II.18], $P_l^m(-x) = (-1)^{l-m} P_l^m(x)$.

Very much the same as in earlier $\theta = 0$ case, the dipole field expansion coefficients $\alpha_{\gamma L}^d$ of Eq. (A9) are readily obtained by substituting $h_l^{(1)}$ for j_l in the above expressions (A15), (A16).

In virtue of [46, 10.53.1], the only nonzero Bessel terms in the limit $r_d \rightarrow 0$ in Eq. (A9) are due to

$$j_0(z) \rightarrow 1, \quad \frac{j_1(z)}{z} \rightarrow \frac{1}{3}, \quad j_1'(z) \rightarrow \frac{1}{3!!} \quad (z \rightarrow 0).$$

2. $\delta_S(\mathbf{r}_1, \mathbf{r}_2)$

The orthonormality of vector spherical harmonics $\mathbf{Y}_{lm}^{(c)}$ (see (A.8) of Ref. [25]) implies

$$\text{Tr} \sum_{l=1}^{\infty} \sum_{m=-l}^l \sum_c \mathbf{Y}_{lm}^{(c)}(\mathbf{r}_1) \otimes \mathbf{Y}_{lm}^{(c)*}(\mathbf{r}_2) = 3\delta_S(\mathbf{r}_1, \mathbf{r}_2). \tag{A17}$$

On making use of (A3), one has in $(\hat{\theta}, \hat{\varphi})$ coordinates [cf. Eqs. (105) of Ref. [25]]

$$\begin{aligned}
\mathbf{Y}_L^{(m)}(\mathbf{r}_1) \otimes \mathbf{Y}_L^{(m)*}(\mathbf{r}_2) &= d_l^2 e^{im(\varphi_1 - \varphi_2)} \\
&\times \begin{pmatrix} \pi_{ml}(\theta_1)\pi_{ml}(\theta_2), & -i\pi_{ml}(\theta_1)\tau_{ml}(\theta_2) \\ i\tau_{ml}(\theta_1)\pi_{ml}(\theta_2), & \tau_{ml}(\theta_1)\tau_{ml}(\theta_2) \end{pmatrix}, \\
\mathbf{Y}_L^{(e)}(\mathbf{r}_1) \otimes \mathbf{Y}_L^{(e)*}(\mathbf{r}_2) &= d_l^2 e^{im(\varphi_1 - \varphi_2)} \\
&\times \begin{pmatrix} \tau_{ml}(\theta_1)\tau_{ml}(\theta_2), & -i\tau_{ml}(\theta_1)\pi_{ml}(\theta_2) \\ i\pi_{ml}(\theta_1)\tau_{ml}(\theta_2), & \pi_{ml}(\theta_1)\pi_{ml}(\theta_2) \end{pmatrix}.
\end{aligned}$$

Because

$$\begin{aligned}
\mathbf{Y}_L^{(o)}(\mathbf{r}_1) \otimes \mathbf{Y}_L^{(o)*}(\mathbf{r}_2) \\
= l(l+1) d_l^2 e^{im(\varphi_1 - \varphi_2)} d_{0m}^l(\theta_1) d_{0m}^l(\theta_2) \mathbf{r}_1 \otimes \mathbf{r}_2,
\end{aligned}$$

substituting the above relations into (A17) yields

$$\begin{aligned}
&\sum_{l=1}^{\infty} \sum_{m=-l}^l d_l^2 e^{im(\varphi_1 - \varphi_2)} [2\pi_{ml}(\theta_1)\pi_{ml}(\theta_2) \\
&+ 2\tau_{ml}(\theta_1)\tau_{ml}(\theta_2) + l(l+1) d_{0m}^l(\theta_1) d_{0m}^l(\theta_2)] \\
&= 3\delta_S(\mathbf{r}_1, \mathbf{r}_2). \tag{A18}
\end{aligned}$$

In virtue of

$$\sum_{l=1}^{\infty} \frac{2l+1}{4\pi} \sum_{m=-l}^l d_{0m}^l(\theta_1) d_{0m}^l(\theta_2) e^{im(\varphi_1 - \varphi_2)} = \delta_S(\mathbf{r}_1, \mathbf{r}_2), \tag{A19}$$

or that the scalar spherical harmonics,

$$Y_{lm}(\theta, \phi) = (-1)^m \sqrt{\frac{2l+1}{4\pi}} d_{0m}^l(\theta) e^{im\phi},$$

are orthonormal, Eq. (A18) signifies both (A19) and that

$$\begin{aligned}
&\sum_{l=1}^{\infty} \sum_{m=-l}^l d_l^2 e^{im(\varphi_1 - \varphi_2)} [\pi_{ml}(\theta_1)\pi_{ml}(\theta_2) + \tau_{ml}(\theta_1)\tau_{ml}(\theta_2)] \\
&= \delta_S(\mathbf{r}_1, \mathbf{r}_2). \tag{A20}
\end{aligned}$$

Eq. (A19) is obviously compatible with the sum rule

$$\sum_{m=-l}^l (d_{0m}^l)^2 = 1.$$

On selecting $\theta_1 = 0$, while making use of the special values (A5) and (A10), Eq. (A18) can be recast as

$$\begin{aligned}
&\sum_{l=1}^{\infty} \frac{2l+1}{4\pi} \left\{ d_{00}^l(\theta_2) + \frac{1}{\sqrt{l(l+1)}} \sum_{m=\pm 1} e^{im(\varphi_1 - \varphi_2)} \right. \\
&\times [\pi_{ml}(\theta_2) + m\tau_{ml}(\theta_2)] \left. \right\} = 3\delta_S(\mathbf{z}, \mathbf{r}_2),
\end{aligned}$$

where $d_{00}^l(\theta_2) = P_l(\cos \theta_2)$. On making use of

$$\begin{aligned}\pi_{-ml}(\beta) &= (-1)^{m+1} \pi_{ml}(\beta), \\ \tau_{-ml}(\beta) &= (-1)^m \tau_{ml}(\beta),\end{aligned}$$

which follow from the properties of the Wigner functions,

$$\begin{aligned}\sum_{l=1}^{\infty} \frac{2l+1}{4\pi} \left\{ d_{00}^l(\theta_2) + \frac{2 \cos(\varphi_1 - \varphi_2)}{\sqrt{l(l+1)}} [\pi_{1l}(\theta_2) + \tau_{1l}(\theta_2)] \right\} \\ = 3\delta_S(\mathbf{z}, \mathbf{r}_2).\end{aligned}\quad (\text{A21})$$

In particular, on comparing with Eq. (A20),

$$\sum_{l=1}^{\infty} \frac{2l+1}{4\pi} \frac{\cos(\varphi_1 - \varphi_2)}{\sqrt{l(l+1)}} [\pi_{1l}(\theta_2) + \tau_{1l}(\theta_2)] = \delta_S(\mathbf{z}, \mathbf{r}_2).\quad (\text{A22})$$

3. Far-field amplitude matrix

Upon using identities (9.1.23), (10.1.11-12) of Ref. [48] one finds in the asymptotic region of $z \rightarrow \infty$,

$$h_l^{(1)}(z) \sim i^{-l} h_0^{(1)}(z) = i^{-l-1} \frac{e^{iz}}{z},$$

and

$$\frac{d\left(rh_l^{(1)}\right)(kr)}{dr} \sim i \cdot i^{-l-1} e^{ikr}.$$

Therefore, for $r \gg R_N$, Eq. (3) of Ref. [25] implies

$$\begin{aligned}\mathbf{H}_{ML}(k, \mathbf{r}) &\sim i^{-l-1} \frac{e^{ikr}}{kr} \mathbf{Y}_L^{(m)}(\mathbf{r}), \\ \mathbf{H}_{EL}(k, \mathbf{r}) &\sim i^{-l-1} \frac{e^{ikr}}{kr} \left[\frac{\sqrt{l(l+1)}}{kr} \mathbf{Y}_L^{(o)}(\mathbf{r}) + i \mathbf{Y}_L^{(e)}(\mathbf{r}) \right] \\ &\sim i \cdot i^{-l-1} \frac{e^{ikr}}{kr} \mathbf{Y}_L^{(e)}(\mathbf{r}),\end{aligned}$$

and

$$\begin{aligned}\mathbf{E}(\mathbf{r}) \sim \mathbf{E}_{\parallel}(\mathbf{r}) &= \sum_L i^{-l-1} \left[D_{ML} \mathbf{Y}_L^{(m)} + i D_{EL} \mathbf{Y}_L^{(e)} \right] \frac{e^{ikr}}{kr} \\ &= \sum_L i^{-l} \left[D_{EL} \mathbf{Y}_L^{(e)} - i D_{ML} \mathbf{Y}_L^{(m)} \right] \frac{e^{ikr}}{kr},\end{aligned}\quad (\text{A23})$$

where, in order to facilitate comparison with Ref. [25], $D_{\gamma L}$'s here correspond to the amplitudes $B_{\gamma L}(N+1)$ in the main text. In general, on using the orthogonality of the vector spherical harmonics in the ordinary vector

sense, one finds from Eq. (A23) in the limit $r \gg R_N$

$$\begin{aligned}|\mathbf{E}(\mathbf{r})|^2 &\sim \frac{1}{(kr)^2} \sum_{LL'} \left[D_{ML} D_{ML'}^* \mathbf{Y}_L^{(m)} \cdot \mathbf{Y}_{L'}^{(m)*} \right. \\ &\quad \left. + D_{EL} D_{EL'}^* \mathbf{Y}_L^{(e)} \cdot \mathbf{Y}_{L'}^{(e)*} \right].\end{aligned}$$

According to Eq. (21) of Ref. [49], the far-field amplitude matrix is defined by

$$\mathbf{F}(\theta, \varphi) = \left. \frac{r \mathbf{E}(\mathbf{r})}{e^{ikr}} \right|_{kr \rightarrow \infty}.$$

On substituting (A23) one finds

$$\mathbf{F}(\theta, \varphi) = \frac{1}{k} \sum_L i^{-l-1} \left[D_{ML} \mathbf{Y}_L^{(m)} + i D_{EL} \mathbf{Y}_L^{(e)} \right],\quad (\text{A24})$$

where $\mathbf{r}/r = (\sin \theta \cos \varphi, \sin \theta \sin \varphi, \cos \theta)$. The knowledge of a far-field amplitude matrix is of crucial importance in determining, e.g. the SERS enhancement factors [49]. Now, irrespective of the dipole position, the expansion coefficient $D_{\gamma L}$ is an m -independent linear combination of the dipole field expansion coefficients $a_{\gamma L}^d$ and $\alpha_{\gamma L}^d$ [cf. Eq. (67) of Ref. [25]],

$$D_{\gamma L} = P_{\gamma l} a_{\gamma L}^d + Q_{\gamma l} \alpha_{\gamma L}^d,$$

where the coefficients $P_{\gamma l}$ and $Q_{\gamma l}$ do not depend on m . The expression, which summarizes in a concise form the results of Eqs. (60), (61), (63), (66) of Ref. [25], makes it obvious that whenever $a_{\gamma L}^d = \alpha_{\gamma L}^d = 0$ for some m , then $D_{\gamma L} = 0$ for the m . According to Eqs. (A12), (A13), (A15), (A16), the vanishing of $a_{\gamma L}^d$ and $\alpha_{\gamma L}^d$ for nearly all m 's occurs for a dipole located on the z -axis. In the latter case, the dipole field expansion coefficients $a_{\gamma L}^d$ (and correspondingly $\alpha_{\gamma L}^d$) are identically zero, unless the angular momentum number $m = 0$ and $m = \pm 1$ for the respective radial and tangential dipole orientations. This makes it possible to simplify the expression (A23).

For the *radial* dipole orientation of a dipole located on the z -axis,

$$\mathbf{E}(\mathbf{r}) \sim \sum_l i^{-l} D_{E10} \mathbf{Y}_{10}^{(e)} \frac{e^{ikr}}{kr}.$$

According to (A3), $\mathbf{Y}_{10}^{(e)} \sim \hat{\theta} \tau_{0l}$ because $\pi_{0l} \equiv 0$ [cf. Eq. (A2)]. On comparing with (A22) one can conclude that the δ -function directivity is *impossible* for the *radial* dipole orientation, irrespective which values of D_{E10} are chosen.

In what follows we show that the δ -function directivity is *possible* for the *tangential* dipole orientation. In the special case of $|m| = 1$, $\mathbf{Y}_L^{(c)*}(\mathbf{r}_d) = -(-1)^m \mathbf{Y}_{l,-m}^{(c)}(\mathbf{r}_d)$ implies $\mathbf{Y}_{l,-1}^{(c)}(\mathbf{r}_d) = \mathbf{Y}_{l,1}^{(c)*}(\mathbf{r}_d)$. Hence, for the *tangential*

dipole orientations of a dipole located on the z -axis,

$$\begin{aligned} \mathbf{E}(\mathbf{r}) &\sim \sum_l i^{-l-1} \sum_{m=\pm 1} \left[D_{Mlm} \mathbf{Y}_{lm}^{(m)} + i D_{Elm} \mathbf{Y}_{lm}^{(e)} \right] \frac{e^{ikr}}{kr} \\ &\sim 2 \sum_l i^{-l} \left[\tilde{D}_{Ml1} \Re \mathbf{Y}_{l1}^{(m)} + i \tilde{D}_{El1} \Im \mathbf{Y}_{l1}^{(e)} \right] \frac{e^{ikr}}{kr}, \end{aligned} \quad (\text{A25})$$

where, in virtue of (A12) and (A15), it has been expedient to factorize $D_{\gamma lm}$ for $m = \pm 1$ on the first line as $D_{Mlm} = i \tilde{D}_{Ml1}$ and $D_{El,\pm 1} = \pm \tilde{D}_{El1}$.

Eventually, on making use of Eqs. (A3) that

$$\begin{aligned} \mathbf{Y}_L^{(m)} &= (-1)^m i d_l \left[i \hat{\theta} \pi_{ml} - \hat{\varphi} \tau_{ml} \right] e^{im\varphi}, \\ \mathbf{Y}_L^{(e)} &= (-1)^m i d_l \left[\hat{\theta} \tau_{ml} + i \hat{\varphi} \pi_{ml} \right] e^{im\varphi}, \end{aligned}$$

one finds

$$\begin{aligned} \Re \mathbf{Y}_{l1}^{(m)} &= d_l \Im [\mathbf{C}_L(\theta) e^{i\varphi}] \\ &= d_l \{ \Im [\mathbf{C}_L(\theta)] \cos \varphi + \Re [\mathbf{C}_L(\theta)] \sin \varphi \} \\ &= d_l \{ \hat{\theta} \pi_{1l} \cos \varphi - \hat{\varphi} \tau_{1l} \sin \varphi \}, \\ \Im \mathbf{Y}_{l1}^{(e)} &= -d_l \Re [\mathbf{B}_L(\theta) e^{im\varphi}] \\ &= -d_l \{ \Re [\mathbf{B}_L(\theta)] \cos \varphi - \Im [\mathbf{B}_L(\theta)] \sin \varphi \} \\ &= -d_l \{ \hat{\theta} \tau_{1l} \cos \varphi - \hat{\varphi} \pi_{1l} \sin \varphi \}. \end{aligned}$$

Hence one finds in (A25) only linear combinations of $\hat{\theta} \cos \varphi$ and $\hat{\varphi} \sin \varphi$ dependencies,

$$\begin{aligned} \mathbf{E}(\mathbf{r}) &\sim 2 \sum_l i^{-l} d_l \left\{ \hat{\theta} \cos \varphi \left(\tilde{D}_{Ml1} \pi_{1l} - i \tilde{D}_{El1} \tau_{1l} \right) \right. \\ &\quad \left. + \hat{\varphi} \sin \varphi \left(-\tilde{D}_{Ml1} \tau_{1l} + i \tilde{D}_{El1} \pi_{1l} \right) \right\} \frac{e^{ikr}}{kr}. \end{aligned} \quad (\text{A26})$$

In what follows we shall demonstrate that one can, in principle, achieve the δ -function directivity for $\theta = 0$ direction (i.e. along the positive z -axis where the dipole is located), provided that the initial D -coefficients (i.e. without a tilde) satisfy [cf. (A21)]

$$D_{Ml1} = D_{El1} \sim i^l \left(\frac{2l+1}{4\pi} \right)^{1/2}. \quad (\text{A27})$$

With (A27) substituted back into (A26), while taking into account the expression [25, (A.6)] for d_l ,

$$\begin{aligned} \mathbf{E}(\mathbf{r}) &\sim 2 \sum_l \left[\frac{2l+1}{4\pi l(l+1)} \right]^{1/2} \left(\frac{2l+1}{4\pi} \right)^{1/2} \times \\ &\quad \left\{ -i \hat{\theta} \cos \varphi (\pi_{1l} + \tau_{1l}) + i \hat{\varphi} \sin \varphi (\tau_{1l} + \pi_{1l}) \right\} \frac{e^{ikr}}{kr} \\ &\sim \frac{i}{2\pi} \sum_l \frac{2l+1}{\sqrt{l(l+1)}} (\pi_{1l} + \tau_{1l}) \left(-\hat{\theta} \cos \varphi + \hat{\varphi} \sin \varphi \right) \frac{e^{ikr}}{kr}. \end{aligned}$$

On comparing with (A22), one immediately recognizes an angular δ -function in the terms proportional to $\hat{\theta}$ and $\hat{\varphi}$. The latter can be exemplified on making use of the special values (A10) for $\theta = 0$,

$$\mathbf{E}(\mathbf{r}) \sim \frac{i}{2\pi} \left[\left(-\hat{\theta} \cos \varphi + \hat{\varphi} \sin \varphi \right) \frac{e^{ikr}}{kr} \right] \sum_l (2l+1),$$

which leads to

$$|\mathbf{E}(\mathbf{r})|^2 \sim \frac{1}{(2\pi kr)^2} \left| \sum_l (2l+1) \right|^2. \quad (\text{A28})$$

The directivity is defined as

$$D = \frac{4\pi r^2 |\mathbf{E}(\mathbf{r})|^2}{r^2 \oint |\mathbf{E}(\mathbf{r})|^2 d\Omega}. \quad (\text{A29})$$

The surface integral of the modulus of (A25) can be performed straightforwardly on using the orthonormality (A.7) of Ref. [25] of the vector spherical harmonics $\mathbf{Y}_L^{(a)}$,

$$r^2 \oint |\mathbf{E}(\mathbf{r})|^2 d\Omega = \sum_l \frac{4(2l+1)}{4\pi k^2} = \frac{1}{\pi k^2} \sum_l (2l+1), \quad (\text{A30})$$

where we have substituted expressions (A27) for D_{Ml1} and D_{El1} in (A25). Therefore, on combining the results (A28) and (A30) into (A29), the maximum directivity is (cf. [34, Eq. (8)])

$$\begin{aligned} D_{\max} &= \frac{|\sum_l (2l+1)|^2}{\pi k^2 \frac{\sum_l (2l+1)}{\pi k^2}} = \frac{|\sum_l (2l+1)|^2}{\sum_l (2l+1)} \\ &= \sum_{l=1}^{l_{\max}} (2l+1) = (l_{\max} + 1)^2 - 1 \\ &= l_{\max}(l_{\max} + 2), \end{aligned} \quad (\text{A31})$$

provided a cutoff l_{\max} on the summation over l is imposed. Obviously, with each increasing l_{\max} one has to satisfy simultaneously more conditions (A27) in order to attain the above D_{\max} value. Analogous to the cylindrical antenna case of Ref. [34], this can be only achieved by increasing gradually the number of shells, because each shell provides a new set of parameters necessary to satisfy the increased number of conditions (A27). Only then a spherical analog of the δ -function directivity in the cylindrical case [34, Eq. (5)] can be achieved. For $\theta = \pi$ direction mutatis mutandis analogous applies, provided that the prefactor i^l in (A27) is amended to $(-i)^l$, in order to accommodate the extra factor $-(-1)^l$ in (A15) relative to (A12).

Appendix B: Optimization of a homogeneous sphere

In this part, we discuss a simple optimization strategy for electrically small antenna to get design with the desired directivity. Only dipole excitation of an electrically small spherical antenna is considered here, but this approach can subsequently be developed for other sources of excitation and scatterer geometries.

Since $r_{lp} \sim \eta_{lp} k R_1$ is a quite good approximation for a resonance condition with high refractive index (see Fig. B1), this linking relationship between resonance conditions of the homogeneous sphere with the roots r_{lp} of the Bessel function j_l can be used to narrow the search area during optimization. Optimization is needed to find exact dipole position and refractive index of the scatterer. Optimum dipole position for resonances with $l \leq 1$ is located either inside or outside the outer layer and for resonances with $l > 1$ it is located either inside or in close proximity to the outer layer and with increase in p it tends either to the sphere origin or to the outer surface. However, the resonances with fixed l and p have their characteristic dipole position.

Let us consider a sphere with a fixed $R_1/\lambda = 0.005$ and require directivity to be higher than 10. From Figure 1(a) one can see that the refractive index which provide such directivity is $\eta_1 \simeq \eta_{132}$ (see Table I):

$$\eta_{132} = \frac{r_{32}}{kR_1} = \frac{10.4171}{2\pi \cdot 0.005} = 331.587$$

For the fixed size parameter $kR_1 = 2\pi \cdot 0.005$ there are only two optimized parameters:

- refractive index
 $\eta_1 = 0.999\eta_{132} \dots 1.001\eta_{132}$;
- dimensionless dipole position
 $kr_d = 0.001kR_1 \dots 1.5kR_1$.

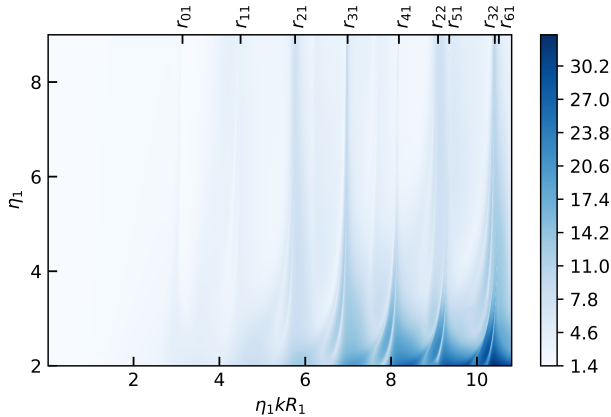


FIG. B1. Optimized directivity D_{max} of a homogeneous spherical antenna excited by a point electric dipole source as a function of the size parameter $\eta_1 k R_1$ and refractive index η_1 .

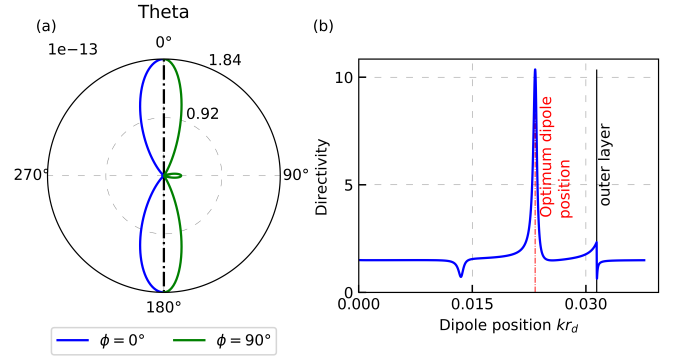


FIG. B2. Optimized design of a spherical scatterer with $kR_1 = 2\pi \cdot 0.005$ and $\eta \simeq \eta_{132}$ excited by a single point dipole at the position $kr_d = 0.0233$: (a) Far field distribution; (b) Dependence of directivity on the dipole position.

The higher the refractive index, the narrower the search area can be. Optimized design is shown in Fig. B2.

Directivity value $D_{max} = 10.357$ can be achieved with dipole located inside the sphere (Fig. B2(b)). The directivity result for the considered example does not depend so much on the dipole position (3 significant digits), but rather on the refractive index (8 significant digits) to maintain the calculation accuracy up to 0.1%.

Obtained refractive index $\eta_1 = 331.58684$ is close to the initial assumption $\eta_{132} = 331.587$. The deviation of various assumed η_{lp} for $kR = 0.005$ is $< 0.01\%$. Dimensionless dipole position for the considered example is $kr_d = 0.0233$.

In a similar way one can find other directive designs for a sphere with $kR_1 = 2\pi \cdot 0.005$ (see Table B1).

| η_{lp} | η_1 | r_d/R_1 | D_{max} |
|---------------------------|------------|-----------|-----------|
| $\eta_{111} = 143.029$ | 143.0116 | 1.2 | 4 |
| $\eta_{121} = 183.458$ | 183.456604 | 1 | 7.5 |
| $\eta_{131} = 222.432$ | 222.43183 | 0.643 | 9.45 |
| $\eta_{112} = 245.902$ | 245.89719 | 1.8 | 4 |
| $\eta_{141} = 260.459$ | 260.45907 | 0.67 | 7 |
| $\eta_{122} = 289.503$ | 289.50302 | 1.02 | 7.5 |
| $\eta_{151} = 297.804$ | 297.80408 | 0.48 | 8.56 |
| $\eta_{132} = 331.587$ | 331.58684 | 0.742 | 10.36 |
| ... | ... | ... | ... |
| $\eta_{133} = 436.02$ | 436.02141 | 0.796 | 10.46 |
| $\eta_{134} = 538.696$ | 538.69544 | 0.831 | 10.50 |
| $\eta_{135} = 640.497$ | 640.49686 | 0.856 | 10.52 |
| ... | ... | ... | ... |
| $\eta_{13(15)} = 1646.31$ | 1646.30662 | 1.0001 | 11.21 |

TABLE B1. Optimization results for $kR_1 = 2\pi \cdot 0.005$.

It is worth noting that for resonances with any fixed $l \geq 1$ and increasing p , an optimal dipole position gradually tends either to the outer surface or to the sphere origin.

Appendix C: Superdirective designs

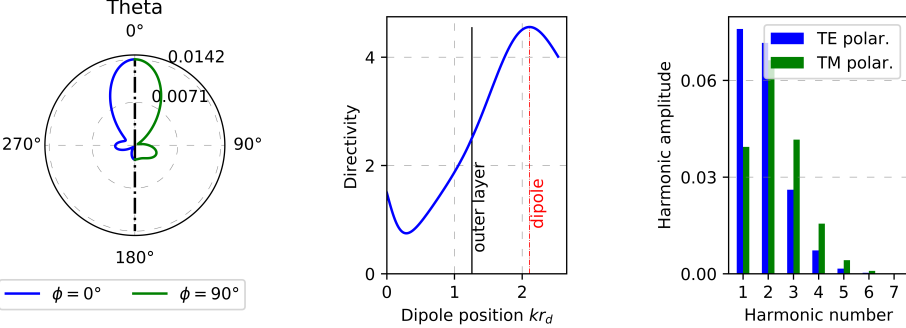
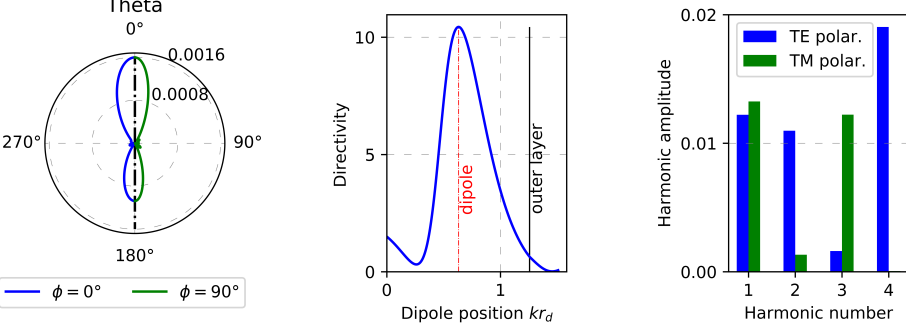
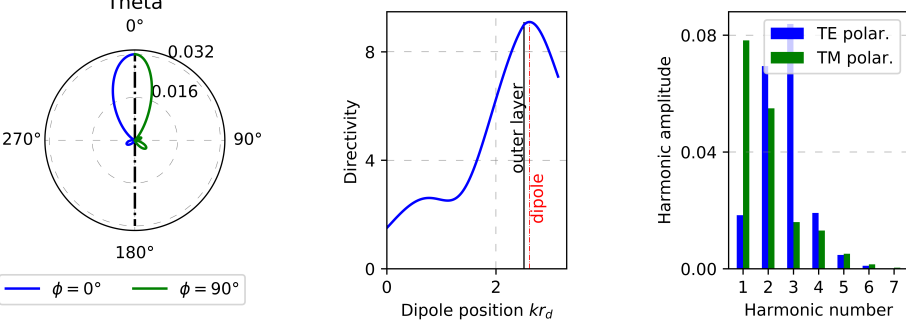
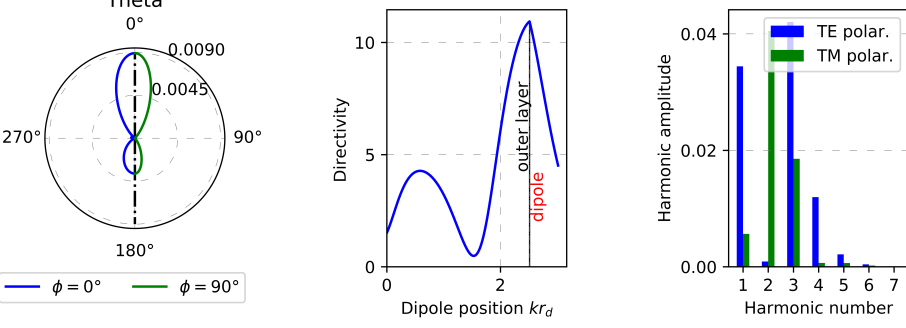
| № | Radiation patterns, directivity dependence and harmonic amplitudes | Optimized parameters |
|-----|---|---|
| 1.1 |  <p>Theta 0° 270° 180° 90°</p> <p>— $\phi = 0^\circ$ — $\phi = 90^\circ$</p> <p>Directivity</p> <p>Dipole position kr_d</p> <p>Harmonic amplitude</p> <p>Harmonic number</p> | $D_{max} = 4.56,$ $kr_d = 2.109,$ $kR_1 = 0.4\pi,$ $\eta_1 = 2.4$ |
| 1.2 |  <p>Theta 0° 270° 180° 90°</p> <p>— $\phi = 0^\circ$ — $\phi = 90^\circ$</p> <p>Directivity</p> <p>Dipole position kr_d</p> <p>Harmonic amplitude</p> <p>Harmonic number</p> | $D_{max} = 10.44,$ $kr_d = 0.6323,$ $kR_1 = 0.4\pi,$ $\eta_1 = 5.5265$ |
| 1.3 |  <p>Theta 0° 270° 180° 90°</p> <p>— $\phi = 0^\circ$ — $\phi = 90^\circ$</p> <p>Directivity</p> <p>Dipole position kr_d</p> <p>Harmonic amplitude</p> <p>Harmonic number</p> | $D_{max} = 9.1,$ $kr_d = 2.6165,$ $kR_1 = 0.8\pi,$ $\eta_1 = 1.87$ |
| 1.4 |  <p>Theta 0° 270° 180° 90°</p> <p>— $\phi = 0^\circ$ — $\phi = 90^\circ$</p> <p>Directivity</p> <p>Dipole position kr_d</p> <p>Harmonic amplitude</p> <p>Harmonic number</p> | $D_{max} = 10.94,$ $kr_d = 0.8\pi,$ $kR_1 = 0.8\pi,$ $\eta_1 = 2.313$ |

TABLE C1. Examples of superdirective designs for a homogeneous sphere after optimization with a constraint on the size parameter $kr_1 \leq kr_{max}$ and on the continuously varying refractive index $1 \leq \eta_1 \leq \eta_{max}$

| № | Radiation patterns, directivity dependence and harmonic amplitudes | Optimized parameters |
|-----|--|---|
| 2.1 | | $D_{max} = 13.6,$ $kr_d = 0.315,$ $kR_1 = 0.07,$ $kR_2 = 0.2957978,$ $\eta_1 = 16.673333,$ $\eta_2 = 27.658633,$ |
| 2.2 | | $D_{max} = 4.6,$ $kr_d = 1.19381,$ $kR_1 = 0.4359,$ $kR_2 = 1.0283,$ $kR_3 = 1.19381,$ $\eta_1 = 1,$ $\eta_2 = 3.2462,$ $\eta_3 = 2.8956$ |
| 2.3 | | $D_{max} = 80.3,$ $kr_d = 5.6924,$ $kR_1 = 2.865,$ $kR_2 = 5.081,$ $kR_3 = 6.9115,$ $\eta_1 = 2.203,$ $\eta_2 = 2.3008,$ $\eta_3 = 2.48168$ |

TABLE C2. Examples of superdirective designs for a multilayer sphere after optimization with a constraint on the size parameter $kR_n \leq kR_{max}$ and on the continuously varying refractive index $1 \leq \eta_n \leq \eta_{max}$.

Examples of optimized designs of dipole-excited superdirective spherical antennas are provided in Tables C1 and C2. Table C1 demonstrates several optimized designs for a homogeneous sphere with different refractive indices and size parameters ($R/\lambda \leq 0.2$ for examples 1.1 and 1.2, $R/\lambda \leq 0.4$ for examples 1.3 and 1.4), table C2 contains several optimized designs for a multilayer sphere. The second column in both tables demonstrates far-field radiation pattern, dependence on the dipole position for the considered example and the absolute values of the harmonic amplitudes for the case of maximum directivity. The far-field pattern of a spherical scatterer is axially symmetric, therefore two different planes are combined into one plot: the left half shows the plane containing the dipole vector, \mathbf{p} , and the z -axis ($\varphi = 0^\circ$), the right half describes the perpendicular plane ($\varphi = 90^\circ$).